International Journal of Fatigue, Volume 32, Issue 7, July 2010, Pages 1180-1189

Accepted Manuscript

Fatigue Crack Growth Behaviour and Life Prediction for 2324-T39 and 7050-T7451 Aluminium Alloys under Truncated Load Spectra

Rui Bao, Xiang Zhang

PII: S0142-1123(09)00361-2
DOI: 10.1016/j.ijfatigue.2009.12.010
Reference: JIJF 2401

To appear in: *International Journal of Fatigue*

Received Date: 17 September 2009
Revised Date: 14 December 2009
Accepted Date: 21 December 2009

Please cite this article as: Bao, R., Zhang, X., Fatigue Crack Growth Behaviour and Life Prediction for 2324-T39 and 7050-T7451 Aluminium Alloys under Truncated Load Spectra, *International Journal of Fatigue* (2009), doi: 10.1016/j.ijfatigue.2009.12.010

This is a PDF file of an unedited manuscript that has been accepted for publication. As a service to our customers we are providing this early version of the manuscript. The manuscript will undergo copyediting, typesetting, and review of the resulting proof before it is published in its final form. Please note that during the production process errors may be discovered which could affect the content, and all legal disclaimers that apply to the journal pertain.

ACCEPTED MANUSCRIPT

Fatigue Crack Growth Behaviour and Life Prediction for 2324-T39 and 7050-T7451 Aluminium Alloys under Truncated Load Spectra

Rui Bao[1*], Xiang Zhang[2]

[1]Institute of Solid Mechanics, School of Aeronautic Science and Engineering, Beihang University (BUAA), Beijing, 100191, China

[2]Department of Aerospace Engineering, School of Engineering, Cranfield University, Bedford, MK43 0AL, U.K.

Abstract: This paper presents a study of crack growth behaviour in aluminium alloys 2324-T39 and 7050-T7451 subjected to flight-by-flight load spectra at different low-stress truncation levels. Crack branching was observed in the higher truncation levels for the 2324 and in all truncation levels for the 7050. Mode-I crack growth life can be predicted for the 2324 alloy by the NASGRO equation and the Generalised Willenborg retardation model. However, quantitative prediction of the fatigue life of a significantly branched crack is still a problem. Material properties, test sample's orientation and applied stress intensity factor range all play dominant roles in the fracture process.

Keywords: Fatigue crack growth, fatigue load spectra, crack branching, retardation, life prediction.

Nomenclature

a, a_0	Half crack length, initial half crack length in middle-crack tension, M(T), specimen

* Corresponding author. Tel.: +86 10 82338663.
Email address: rbao@buaa.edu.cn (R.Bao)

ACCEPTED MANUSCRIPT

C, n, p, q	Material constants in the NASGRO fatigue crack growth rate law
C_{f0}	Parameter in AFGROW crack closure model
da/dN	Crack growth rate
E	Young's modulus
f	Parameter in NASGRO equation taking account of the crack closure effect
K, $K_{\max}$	Stress intensity factor (SIF), maximum SIF
ΔK, ΔK_{th}	SIF range, SIF threshold
K_{crit}	Apparent fracture toughness
N	Number of cycles in crack growth laws and NASGRO equation
N_f	Fatigue crack growth life in terms of flights
R	Nominal stress intensity factor ratio ($R = K_{min}/K_{max} = \sigma_{min}/\sigma_{max}$)
SOR	Shut-off Ratio in Willenborg retardation model

1. Introduction

For the damage tolerance design of aircraft structures, fatigue tests are required at all structural levels according to the airworthiness regulations [1] to support and validate the crack growth life predictions. There are several aspects in both the practical fatigue testing and the development of predictive models.

Since a representative service loading spectrum can contain a large number of low amplitude load cycles that do not cause fatigue damage but consume unacceptable testing time and cost in the full scale fatigue tests (FSFT), an economic and common practice is to eliminate these low amplitude stress cycles in the test spectrum. Tests and analysis on laboratory specimens are necessary to determine an acceptable load truncation level for the FSFT of a structural component. These laboratory sample tests are used to demonstrate that the elimination of

ACCEPTED MANUSCRIPT

certain low-range loads will not change the characteristic of the crack growth and have little influence on crack growth life while considering the scale of time saving.

The second aspect is the requirement of life prediction tools. Fatigue crack growth (FCG) behaviour and life prediction methods under the constant amplitude loads (CAL) have been well established for commonly used aluminium alloys. The problem of predicting FCG life under the variable amplitude loads (VAL) is still challenging due to the load sequence and load interaction effects [2, 3]. For simple VAL sequences, e.g. large numbers of CAL cycles plus occasional tensile overload cycles, or an overload followed by an underload, current prediction methods include the Wheeler [4], the Generalised Willenborg [5, 6], and the crack closure models [7, 8]. These models and a few others have now been implemented in computer packages, such as the AFGROW crack growth analysis code [8]. However, the problem of life prediction gets more complex when randomly ordered flight-by-flight loading spectrum is used. In most of the cases, the low-amplitude load cycles that tend to be eliminated contribute little to the fatigue crack growth. However, for some circumstances, the elimination of small load cycles might shift the balance between the crack initiation and crack growth phases [9]. Moreover, the overload retardation effect is found to be very sensitive to subsequent underload cycles [2, 10, 11] as well as to the cycle numbers of subsequent lower amplitude stresses [10].

Thirdly, the influence of the low-amplitude load cycles on crack growth rates also depends on the material properties and test sample's material orientation. In the last four decades, most research efforts in the aircraft applications have been focused on the 2024 and 7075 aluminium alloys (AA). Consequently, adequate crack growth prediction models are now available [12]. In recent years, trend in the aircraft industry is to gradually introduce new versions of the 2000 and the 7000 series alloys due to their superior mechanical properties. Their performance in terms of FCG life in flight-by-flight loads needs to be investigated.

ACCEPTED MANUSCRIPT

The materials investigated in this study are the AA 2324-T39 and AA 7050-T7451, which are widely employed in the current generation of aircraft components. The former is a higher strength version of AA 2024-T351 and is a high-purity controlled composition variant of 2024, and is mainly applied on the lower wing skin and center wing box components of new commercial transport aircraft. The fracture behavior and crack growth behavior of 2324 have been widely investigated in recent years for better understanding and further application of this material [13]. Alloy 7050 is the premier choice for aerospace applications requiring the best possible combination of strength, stress corrosion cracking (SCC) resistance and toughness. However, it is one of these highly anisotropic alloys; consequently, crack growth behaviour along the short transverse direction (L-S) is found to be quite different from that along the long transverse direction (L-T). Nevertheless, the L-S orientated plates have found some applications in the spar caps and stringer webs of machined integral skin-stringer panels. Progress has been made in understanding the crack growth behaviour in L-S orientated AA 7050-T7451 plates under CAL at different stress ratios [14, 15], in which comparisons of the failure modes between the L-S and T-L plates under truncated loading spectra are also presented. Small crack growth rates in AA 7050-T7451 subjected to simple load sequences containing underloads are reported in [16] to generate constant amplitude crack growth data for use in life predictions.

The experimental tests conducted in this study were designed to achieve two objectives: 1) to select a suitable low-load truncation level for the FSFT; 2) to investigate the characteristics of crack growth behavior under different load spectra with various truncation levels. The first objective was achieved and reported in [17]. The purpose of this paper is to present the investigation findings towards the second objective, which covers the studies of crack growth behaviour under a flight-by-flight loading spectrum of a civil transport aircraft wing at

ACCEPTED MANUSCRIPT

different small-stress range truncation levels and the performance of current predictive models in spectrum loads.

2. Experimental procedures

2.1 Material

Crack propagation tests were conducted using the middle-crack tension, M(T), specimens made of AA 2324-T39 and AA 7050-T7451. The configuration and orientation of the specimens are shown in Fig. 1 and Table 1. The material data is found in reference [18,19]. For alloy 2324, (WT.%), Si 0.1, Fe 0.12, Cu 3.8-4.4, Mn 0.3-0.9, Mg 1.2-1.8, Cr 0.10, Zn 0.25, Ti 0.15, others each 0.05, others total 0.15, Aluminum Remainder. For alloy 7050, (WT.%), Si 0.12, Fe 0.15, Cu 2.0-2.6, Mn 0.10, Mg 1.9-2.6, Cr 0.04, Zn 5.7-6.7, Zr 0.08-0.115, Ti 0.06, others each 0.05, others total 0.15, Balance Aluminum. The mechanical properties are fully defined in [18, 19] and presented in Table 2. Crack growth rate and fatigue properties are available for the L-T orientation (refer to Fig. 1) for both alloys [20].

A total of 66 specimens were tested; for each load truncation level six specimens were tested for AA 2324-T39 and five specimens for AA 7050-T7451.

2.2 Load spectra

The baseline load spectrum is a flight-by-flight spectrum with each load block simulating 4200 flights. The gust and manoeuvres loads are represented by ten load levels flatulating around the mean load corresponding to 1g flight condition. The flights in each load block are classified into five types, stated as A, B, C, D and E, respectively, according to the stress levels. Flight type A is the most severe loading condition occurring only once in each block, whereas flight type E is the least severe occurring 2958 times in each block. The five flight types were arranged randomly within one block except that flight type A was arranged to

ACCEPTED MANUSCRIPT

occur near the middle and in the second half of a block. The taking-off and landing taxiing loads were taken into account by eight equivalent loading cycles in each flight. Fig. 2(a) illustrates a loading segment of the baseline spectrum containing the flight types A, B and E. It can be seen that the spectrum is dominated by tension loads.

The baseline spectrum (S0) was filtered by removing small stress range cycles to obtain different truncated spectra, while the taxiing loads during each flight were retained. A 9.82% truncation level indicates that those load cycles with stress range less than 9.82% of the maximum stress range in the S0 were removed, while the other parts of the spectrum were kept unchanged. So no matter what the load truncation level is, the mean stress level remains to correspond to the 1g acceleration. There are five truncation levels resulting in five different truncated load spectra, named as S1, S2, S3, S4 and S5, shown in Table 3. Fig. 2(b) shows the load sequences of flight type A in S0 and S5.

2.3 Fatigue testing

Pre-cracking was accomplished under constant amplitude load of $\sigma_{\max} = 90$ MPa, $R = 0.06$ which resulted in an initial half crack length a_0 of about 5.5 mm. The FCG tests were subsequently carried out under the aforementioned six load spectra until the half crack length a was greater than 24 mm.

All the tests were conducted using the MTS 880 fatigue test system. Specimens were held in a pair of 100 mm wide hydraulic wedge grips.

An observation system consisting of a digital microscope, servo motor and raster ruler was used to record the crack tip position. Incremental crack length measurements were made on both the right and left sides of the front surface of the specimen. The following rules were adopted when recording the crack length: (1) If it is an ideal mode I crack, which is perpendicular to the applied loads and propagating along the *x*-axis, the crack length is the

ACCEPTED MANUSCRIPT

true distance from the symmetric axis of the specimen to the crack tip, Fig. 3(a); (2) If the crack has deviated from the horizontal *x*-axis, then the crack length refers to the projected length of the crack on the *x*-axis, Fig. 3(b); (3) If the crack has branched, the recorded crack length is the projected length of the longest branch, Fig. 3(c).

3. Prediction method

3.1 Review of available crack growth prediction models

Based on the principle of the linear elastic fracture mechanics (LEFM), FCG rates can be correlated with the stress intensity factor range ΔK. There are many empirical FCG laws to describe this relationship. Paris law [21] is the first and most popular, which correlates crack growth rate $\mathrm{d}a/\mathrm{d}N$ with only the ΔK. During the following decades, modifications to the Paris law have been developed by taking into account of different factors. For example, the Forman [22] and Walker equations [23] were proposed to encompass the mean stress effect. Both the Paris and Walker equations work well for the stable crack growth stage showing good linearity in double logarithm coordinate of $\mathrm{d}a/\mathrm{d}N$ vs. ΔK. The Forman equation [22] also introduces the parameter of critical stress intensity factor K_c therefore can be applied in the prediction of the final fracture regime. Hartman and Schijve [24] suggested a modified form of Paris law by adding a parameter of stress intensity threshold which depended strongly on the alloy and the environment. The NASGRO equation [8] takes account of the influences of the mean stress, the critical and threshold SIF, and plasticity-induced crack closure by introducing several empirical constants. Most of the empirical constants in the above mentioned crack growth laws are obtained by fitting measured crack growth test data under constant amplitude stresses.

ACCEPTED MANUSCRIPT

When variable amplitude loading is applied, crack growth behaviour shows more complicated characters. One of the most important factors that should be taken into account is the profound overload retardation effect [2, 12]. However, this effect is much reduced when the tension overload is immediately followed by compressive underload [2, 12]. Furthermore, if a load history has peak loads with a long recurrence period, i.e. peak overload cycle is followed by large numbers of baseline stress cycles, it will result in large retardation in the crack growth curve, while an almost regular crack growth curve may be resulted by a load history which has peak loads with a short recurrence period [10]. These two factors were paid more attention in this study, since the loading spectra in this study all contain a tensile overload in the flight type A which is followed by a negative underload, and with the increase of load truncation levels, the recurrence periods between the two overload peaks become shorter and shorter.

A number of crack growth models have been developed to account for the load interaction effects and thereby enable predictions of crack growth lives. Most of the retardation models are based on either the crack tip plastic zone concept or the crack closure argument. Five retardation models are available in the crack growth prediction software AFGROW; they are the Closure model [7, 8], the FASTRAN model [25], the Hsu [26], Wheeler [4] and Willenborg models [5, 6]. Each retardation model has one or more user adjustable parameter(s), which are used to tune the model to fit the actual test data. Ideally, the parameter in crack retardation models should be a material constant, which is independent of other variables such as the spectrum sequence or load level. The Generalised Willenborg model is a modified version of the original Willenborg model. Physical arguments were used to account for the reduction of the overload retardation due to subsequent underloads. The AFGROW code has adapted the treatment of the underload acceleration effect by using the Chang's model [8, 27] to adjust the overload induced yield zone size. Therefore the effect of

ACCEPTED MANUSCRIPT

compressive stresses after a tension overload is considered. This model is suitable to the overload/underload pattern found in the load spectra used in this study as shown in Fig. 2(b). The AFGROW Closure model is based on the original Elber's crack closure concept [7] and developed by Harter et al. [8]. This type of crack closure models has been very popular in both the constant and variable amplitude loads because they correlate crack growth rates with the effective stress intensity factor range, which is affected by the applied loads and crack opening displacements; both can be related to the cyclic plasticity effect. The AFGROW Closure model uses a single adjustable parameter (C_{f0}) that is determined at stress ratio $R = 0$ in order to "tune" the closure model for a given material. The suggested C_{f0} value by AFGROW for aluminium alloys is 0.3 [8].

3.2 Crack growth and retardation laws used in this study

In this study, FCG life predictions were accomplished by using the AFGROW computer package [20] and employing the NASGRO equation [8], eq. (1). Since this equation takes account of the influences of the mean stress, the critical and threshold SIF, and plasticity-induced crack closure, it usually gives more accurate predictions provided that the required material constants are available. The material constants used in the NASGRO equation for commonly used aluminium alloys, including 2324-T39 studied here, are provided in the database of the AFGROW package.

$$\frac{\mathrm{d}a}{\mathrm{d}N} = C\left[\left(\frac{1-f}{1-R}\right)\Delta K\right]^n \frac{\left(1-\frac{\Delta K_{th}}{\Delta K}\right)^p}{\left(1-\frac{K_{\max}}{K_{crit}}\right)^q} \qquad (1)$$

In order to find a suitable crack retardation model for further analyses of the truncated load spectra, attempts have been made to predict FCG life from a =5.5 mm to 22 mm under the S0 spectrum using the Generalised Willenborg model and Closure model. The prediction results

ACCEPTED MANUSCRIPT

are shown in Table 4. It indicates that both the No-retardation model and the Generalized Willenborg model have achieved good agreement with the test result, whereas the Closure model underestimated the life by 13% using the recommended C_{f0}=0.3. Prediction is found to be sensitive to the value of parameter C_{f0}.

The following crack life predictions are performed by the NASGRO equation (no retardation) and NASGRO equation plus the Generalised Willenborg model.

4. Results and discussion

4.1 Crack growth morphology

4.1.1 AA 2324-T39 L-T oriented specimen

It has been observed during the experiment that cracks subjected to load spectra S0, S1, S2 and S3 are perfect mode I cracks which are flat and straight and perpendicular to the applied loads direction. However, significant crack meandering and/or branching are observed when the low-load range truncation is increased to a certain level, i.e. S4 and S5, shown in Fig. 4. A typical branched crack occurred under spectrum S4 is illustrated in Fig. 5. It is amazing that the crack always tended to grow away from the centerline of the specimen rather than taking a zigzag route.

The crack growth rate dropped significantly after the crack had branched. Some evidence has been found for the relationship between the crack growth path change and the peak stress in the flight type A. This will be discussed in section 4.3. However, branching was not observed immediately after the maximum overload. It can be deduced that the tension overload had introduced a few secondary cracks in the subsurface of the specimen, which were later observed at the surface of the specimen. The lead crack and the secondary cracks kept growing for a period of loading cycles until they were linked up, which has resulted in the

ACCEPTED MANUSCRIPT

observed branched crack. The appearance of the secondary cracks and the linking up process are shown in Fig. 6.

The final failure mode of the branched crack under tension load is almost the same as the perfect mode I crack, showing the typical characteristic of mode I crack in ductile materials, see insert of Fig. 5.

4.1.2 AA 7050-T7451 L-S oriented specimen

Crack turning, meandering, branching and splitting (90^{o} turn) were observed on some specimens whatever the load truncation level was applied as shown in Fig. 7(a). However, not all the specimens showed significant crack turning or branching. It is quit different from the 2324-T39 L-T specimens, in which crack branching occurred only under the spectrum S4 and S5. Schubbe also observed crack branching and splitting in 7050-T7451 L-S oriented specimens [14, 15]. He has pointed out that significant forward growth retardation or splitting is evident at a threshold ΔK value in the range of 10-15 MPa$\sqrt{\text{m}}$ and a distinct crack arrest point where vertical growth is dominating is found when ΔK is between 18 and 20 MPa$\sqrt{\text{m}}$ [14]. In this study, the ΔK value corresponding to the peak stress range in flight type A at initial crack length a_0 =5.5 mm is already above 22 MPa$\sqrt{\text{m}}$, therefore the reason for observed crack branching and splitting is understood, whether or not the load spectrum was truncated. However, it should be mentioned here that slight crack branching was also observed occasionally during the pre-cracking stage with fatigue crack length no more than 0.5 mm from the edge of the saw-cut and $\Delta K < 10$ MPa$\sqrt{\text{m}}$, see Fig. 7(b).

It was hard to get the normal mode I failure strength when performing the residual strength testing after the half crack length a had reached 24 mm. Longitudinal splitting occurred parallel to the load direction, as shown in Fig. 8.

ACCEPTED MANUSCRIPT

4.2 Crack growth lives

Since the loading cycle numbers are different in different load spectra corresponding to different truncation levels, FCG life is defined as the number of flights, N_f, rather than the number of load cycles *N*. Initial half crack length a_0 was 5.5 mm for all the specimens.

Measured a vs. N_f data corresponding to the S0, S2 and S4 load spectra are shown in Fig. 9 (a) and (b) for the two aluminum alloys, which indicate good linearity in the log-linear coordinate. For the clarity of illustration, measured data for spectra S1, S3 and S5 are omitted in these figures. They do follow the same trend and similar scatter range. Fig. 9 (c) and (d) present the best fitted curves of the test data with respect to all the loading spectra using exponential linear least square method, eq. (2),

$$a = Ae^{BN_f} \tag{2}$$

where, *A* and *B* are fitting parameters. Since $a_0 = 5.5$ mm, find $A = 5.5$.

Crack growth retardation due to overload effect are not obvious in this figure for spectra S0, S1, S2, and S3. The significant retardation found in the S4 and S5 spectra tests was partially caused by the crack branching described in section 4.1 and partially by the removal of large numbers of load cycles at these two higher truncation levels.

4.3 Prediction of crack growth lives

Crack growth life predictions were performed using the AFGROW code. Predicted $a \sim N_f$ curves for AA 2324-T39 are shown in Fig. 10. The loading spectra and specimen configuration used in the prediction are the same as those used in the experimental tests. In the figures, “No Retardation” means no load sequence effect was considered; “Willenborg” demotes the Generalized Willenborg model.

ACCEPTED MANUSCRIPT

Following observations can be made: (1) For S0, S1, S2 and S3, i.e. load range truncation level of 0%, 9.82%, 11.72% and 13.98% of the maximum load range, the predicted lives agree well with the test results. (2) Under the spectra S4 and S5, 17.11% and 21.36% truncation levels, measured crack growth lives are much longer than the predicted by Willenborg model. Such differences in the model and measurement cannot be related to the overload retardation effect alone. The main reason is the occurrence of significant crack meandering and branching under these two loading spectra, as mentioned in 4.1, which slow down the lead crack growth rate significantly. This kind of crack growth retardation mechanism is very different from that due to the overload induced plastic zone effect. Crack path deviation was not observed in the tests subjected to load spectra S0, S1, S2 and S3. Hence, the FCG life predictions are fairly accurate, even though the same tensile overloads exist in these spectra as in the S4 and S5. (3) Predicted lives obtained by the "No Retardation" model and "Willenborg" model do not differ from each other too much; both are located within the scatter band of the test data. This is mainly due to the overload pattern: an underload is immediately following the overload, see Fig. 2(b), reducing the retardation effect. Considering the preferred conservativeness in practical applications, NASGRO equation without overload retardation is applicable for such kind of load spectrum investigated in this study with low-stress range truncation levels no higher than 14% of the maximum stress range.

Since the crack growth rate data in terms of $\mathrm{d}a/\mathrm{d}N \sim \Delta K$ is not available for the 7050-T7451 L-S orientation in the AFGROW package, FCG life prediction for this material under spectrum loads was not conducted. Schubbe published some $\mathrm{d}a/\mathrm{d}N \sim \Delta K$ crack growth data for AA 7050-T7451 L-S orientation under constant amplitude loads at different stress ratios in [14]. Attempts have been made to use these data and the Harter T-method to predict crack growth lives for 7050-T7451 under spectrum loads. However, the $\mathrm{d}a/\mathrm{d}N \sim \Delta K$ curves in [14] have a characteristic divergent sinusoidal trend of growth when $\Delta K > 10\ \mathrm{MPa}\sqrt{\mathrm{m}}$, where the

ACCEPTED MANUSCRIPT

growth mode alternates between arrested forward growth and splitting, or arrested vertical growth and continuing forward progression. This crack growth data cannot be used in the crack growth life prediction with the AFGROW, because there is no crack growth model that can take account of such sinusoidal trend of crack growth.

4.4 Crack growth rate

It has been mentioned in section 4.2 that the "No Retardation" option in AFGROW gives good FCG life predictions under the load spectra S0, S1, S2 and S3. However, when the crack branching or splitting occurred under S4 and S5, the observed significant crack growth retardation is not caused by the overload induced yield zone effect; hence it cannot be predicted by these retardation models in AFGROW. Another point is that the crack branching was not observed immediately after the maximum stress in the block. Since it is difficult to observe the overload effect from these $a \sim N_f$ curves, the crack growth rate data may shed light on the effect immediately after each overload. Attempts have been made to find explanations for the relationship between crack growth retardation and tensile overloads.

Fig. 11 shows the measured $da/N_f \sim N_f$ curves for the 2324-T39 L-T and 7050-T7451 L-S specimens under different load truncation levels. Locations of the peak loads in the flight A are marked by the vertical lines. The effect of these peak loads on crack growth rate can be observed. These crack growth rate vs. flights curves show periodic changes in both aluminum alloys. Following observations can be made: (1) The occurrences of crack retardation follow the maximum tension overload regularly in each load block. (2) Retardation is more significant at higher truncation levels, S4 and S5, than that at lower truncation levels, S0, S1, S2 and S3. (3) Crack growth retardation in 2324-T39 L-T specimens is more significant than that in 7050-T7451 L-S specimens, especially with spectra S4 and S5.

ACCEPTED MANUSCRIPT

It is mentioned in 4.1 that crack branching was only observed under spectrum S4 and S5 for the 2324-T39 specimens, but for the 7050-T7451 specimen, crack branching and splitting were observed on almost all the six loading spectra. These observations are also reflected by plots in Fig. 11. Remarkable retardation was also found under S2, S3 for 7050-T7451, especially when the crack became long, as shown in Fig. 11 (b). However, significant retardation can only be seen under S4 and S5 for 2324 alloy in Fig. 11 (a). Referring to Fig. 10(e) and (f) and discussion in section 4.3, currently available crack growth models are incapable of prediction these crack growth morphologies.

Although it can be said from Fig. 10 (a) - (d) that both the "No Retardation" and "Willenborg" model are applicable for 2324-T39 under S0, S1, S2 and S3 spectra, in which no macro-level crack branching was observed, there are still some signs of crack retardation even under the baseline spectrum as shown in Fig. 11 (a); this was predicted by the Willenborg model, Fig. 10 (a)-(d), and the predicted lives are on the conservative side. Fig. 12 shows the "Willenborg" model predicted crack growth rate and comparison with the test measurements of 2324-T39 under S0. It indicates that: (1) Although tension overload was followed immediately by an underload, the crack retardation phenomenon can still be observed during the experiment of AA 2324-T39 under S0 with no crack branching. (2) Although the generalised Willenborg model can predict the crack growth rate in trend, it cannot model precisely the crack retardation introduced by such loading spectrum.

5. Conclusions

(1) Fatigue crack growth tests on AA 2324-T39 L-T and AA 7050-T7451 L-S oriented M(T) specimens under truncated spectrum loading have shown some abnormal behaviours. For the 2324 alloy, crack branching was observed when the low-load range truncation was increased to a certain level. There was no noticeable crack branching under lower truncation levels. For

ACCEPTED MANUSCRIPT

the 7050 L-S specimens, crack branching and slitting were observed in some of the specimens irrespective of the load truncation levels, which means that these are mainly resulted from the test material orientations.

(2) Crack growth life predictions using the AFGROW code have demonstrated that both the NASGRO equation without a retardation model and NASGRO plus the generalised Willenborg retardation model give good predictions for the 2324 alloy under lower stress range truncation levels when there is no significant crack branching; therefore, both models can be employed in crack growth prediction of structural components subjected to these kind of loading spectra. However, all current retardation models derived from the cyclic plasticity argument cannot predict the crack retardation caused by crack branching effect.

(3) Crack growth rate analysis has indicated that the crack growth retardation always followed the peak tensile overload in the spectrum. For the 2324-T39 specimens tested under spectra S0, S1, S2 and S3, these retardations are mainly caused by the crack tip and crack wake plasticity effect, since there is no significant crack branching. For the same specimens tested under higher truncation levels, spectra S4 and S5, retardation effect is more significant which is mainly due to the crack branching. It can be deduced indirectly that the observed crack branching phenomenon has a close relationship with the tensile overload, although it was not observed immediately after the overload.

(4) For the 7050 L-S specimens, the stress intensity factor ranges corresponding to the peak stresses are high enough to cause crack branching and splitting resulting in reduced crack growth rates. With the increasing crack length, peak stress effect on SIF range is even greater, hence crack retardation becomes more significant.

Acknowledgements

ACCEPTED MANUSCRIPT

The authors thank Ms. Hailing Tian at the Shanghai Aircraft Research Institute in China for providing the specimens and load spectra used in this study. They also thank Dr. Jianyu Zhang and all the PhD students in the fatigue and fracture research group at BUAA for helping with the experiments. The National Natural Science Foundation of China is acknowledged for supporting the project (10802003), and finally, R Bao also thanks the China Scholarship Council for offering her the opportunity to visit the Cranfield University where part of this study was performed.

References

[1] Federal Aviation Administration, Advisory Circular - Damage Tolerance and Fatigue Evaluation of Structure, Federal Air Regu-lations 25, AC No.25.271-1C, 1998.

[2] J. Schijve, Fatigue crack propagation in light alloy sheet material and structures, Advances in Aeronautical Sciences, Vol. 3, pp. 387-408. Pergamon Press,1961.

[3] J. Schijve, Fatigue crack growth predictions for variable-amplitude and spectrum loading, Proceedings of Fatigue 87, 1685-1720.

[4] O.E. Wheeler, Spectrum Loading and Crack Growth, Transaction of the ASME, Journal of Basic Engineering, pp. 181-186, March 1972.

[5] J.P. Gallagher, T.F. Hughes, Influence of yield strength on overload affected fatigue crack growth behaviour in 4340 steel, AFFDL-TR-74-28,1974.

[6] J.P. Gallagher, A Generalized Development of Yield-Zone Models, AFFDL-TM-74-28, Air Force Flight Dynamics Laboratory, Wright-Patterson Air Force Base, Ohio, 1974.

[7] W. Elber, The Significance of Fatigue Crack Closure, Damage Tolerance in Aircraft Structures, ASTM STP 486, American Society for Testing and Materials, 1971: 230-242.

ACCEPTED MANUSCRIPT

[8] J. A. Harter, AFGROW users guide and technical manual, AFRL-VA-WP-TR-2006-xxxx, AFGROW, version 4.0011.14, June 2006. Website (accessed July 2008): http://www.siresearch.info/projects/afgrow/downloads/afgrow/download.php.

[9] P. R. Underhill, D.L. DuQuesnay, The effect of dynamic loading on fatigue scatter factor for Al 7050, Int J Fatigue, 30(2008): 614-622.

[10] M. Janssen, J. Zuidema, R. J. H. Wanhill, Fracture Mechanics (2nd edition). Abingdon: Spon Press, 2004.

[11] A. Bacila, X. Decoopman, et al., Study of underload effects on the delay induced by an overload in fatigue crack propagation, Int J Fatigue, 29(2007):1781-1787.

[12] J. Schijve, Fatigue of Structures and materials (2nd Edition), 2009, Springer.

[13] Y. Yamada, J. C. Newman, Crack-closure behavior of 2324-T39 aluminum alloy near-threshold conditions for high load ratio and constant Kmax tests, Int J Fatigue, 31(2009): 1780-1787.

[14] J. J. Schubbe, Fatigue crack propagation in 7050-T7451 plate alloy, Eng Frac Mech, 76(2009): 1037-1048.

[15] J. J. Schubbe, Evaluation of fatigue life and crack growth rates in 7050-T7451 aluminum plate for T-L and L-S oriented failure under truncated spectra loading, Eng Fail Anal, 16(2009): 340-349.

[16] P. White, S. A. Barter, C. Wright, Small crack growth rates from simple sequences containing underloads in AA7050-T7451, Int J Fatigue, 31 (2009) 1865–1874.

[17] H. Tian, R. Bao, J. Zhang, et al., The Influence of Low Load Truncation Level on Crack Growth for Al 2324-T39 and Al 7050-T7451, Chinese Journal of Aeronautics, 22(2009): 401-406.

ACCEPTED MANUSCRIPT

[18] Alcoa Mill Products: 2324 Aluminium Alloy Plate and Sheet; Website (accessed Aug. 2009): http://www.alcoa.com/mill_products/catalog/pdf/alloy2324-t39techsheet.pdf .

[19] Alcoa Mill Products: 7050 Aluminium Alloy Plate and Sheet; Website (accessed Aug. 2009): http://www.alcoa.com/mill_products/catalog/pdf/alloy7050techsheetrev.pdf.

[20] AFGROW – US Air Force Crack Growth Software; V4.12.15.0, 2009.

[21] P. C. Paris, F. Erdogan, A critical analysis of crack propagation laws. Trans, ASME, Series D, Vol. 85(1963): 528-535.

[22] R.G. Foreman, V.E. Kearney and R.M. Engle, Numerical analysis of crack propagation in cyclic-loaded structures, J. Basic Eng. 89 (1967): 459–464.

[23] K. Walker, The Effect of Stress Ratio During Crack Propagation and Fatigue for 2024-T3 and 7075-T6 Aluminum, ASTM STP 462, American Society for Testing and Materials, 1970.

[24] A. Hartman, J. Schijve, The Effects of Environment and Load Frequency on the Crack Propagation Law for Macro Fatigue Crack Growth In Aluminium Alloys, Eng Frac Mech, 1(1970): 615-633.

[25] Newman, J.C., Jr., FASTRAN-II – A Fatigue Crack Growth Structural Analysis Program, NASA TM-104-159, Feb, 1992

[26] Deiters, Thomas, W., "Hsu Model," AFRL-RB-WP-TR-2008-3, May 2008.

[27] J. B. Chang, M. Szamossi, K. W., Liu, Random spectrum fatigue crack life predictions with or without considering load interactions, Methods and Models for Predicting Fatigue Crack Growth under Random Loading, ASTM STP 748, 115-132, 1981.

ACCEPTED MANUSCRIPT

Table 1 Specimen dimensions (mm) and orientation

	Length (L)	Width (W)	Thickness (t)	Half length of the sawcut (a_n)	Orientation
2324-T39	350	98.5	4.5	4	L-T
7050-T7451	350	98.5	6	4	L-S

Table 2 Material mechanical properties

	Tensile Strength (MPa)	Yield Strength (MPa)	Elongation (%)	K_{IC} (plane strain) ($\mathrm{MPa}\sqrt{\mathrm{m}}$)
2324-T39	475	370	8	38.5-44 (t = 19.05-33.02 mm)
7050-T7451	510	441	9	31.9 (L-T), 27.5 (T-L) (t = 25.42 - 50.80 mm)

Table 3 Details of the truncated loading spectra

Name of spectrum	S0	S1	S2	S3	S4	S5
Truncation level (%)	0	9.82	11.72	13.98	17.11	21.36
Cycles eliminated in each block (%)	0	26.56	46.87	62.95	73.35	78.58

Table 4 Predicted FCG life using two different retardation models (spectrum S0, AA 2324-T39)

Model and parameter	No retardation	Closure model		Willenborg model	Test result
		C_{f0}=0.3	C_{f0}=0.5	SOR = 3.0 *	
FCGL (flights)	12739	11755	5517	13729	13495
Error (%)	-5.6	-12.9	-59.1	1.7	----

* SOR=3.0 is recommended by AFGROW technical menu [8] for aluminium alloys.

ACCEPTED MANUSCRIPT

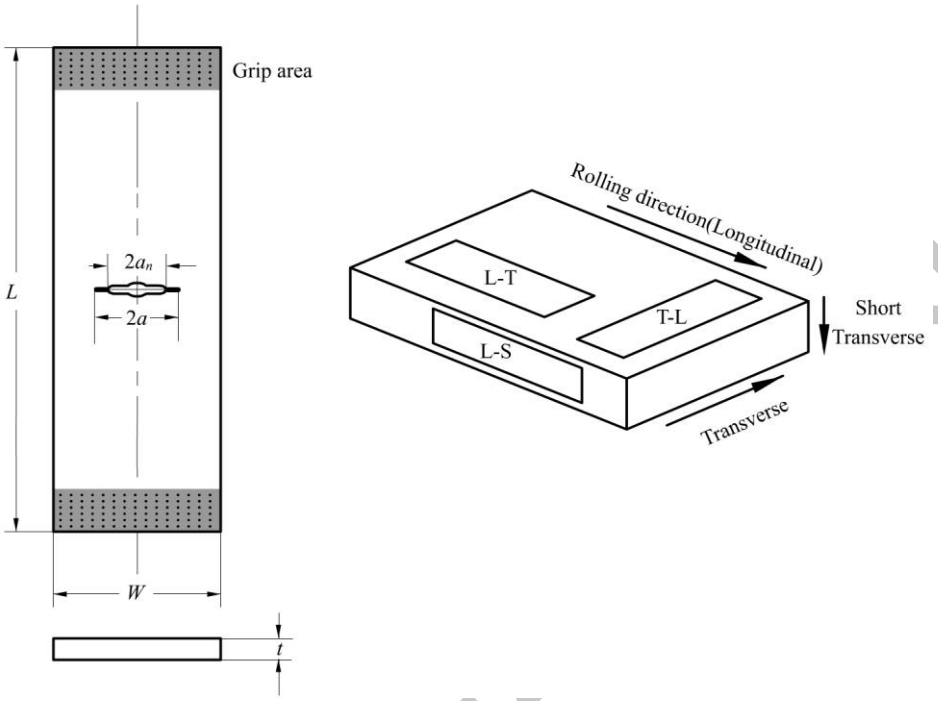

Fig. 1 Configuration of M(T) specimen and definition of material orientation.

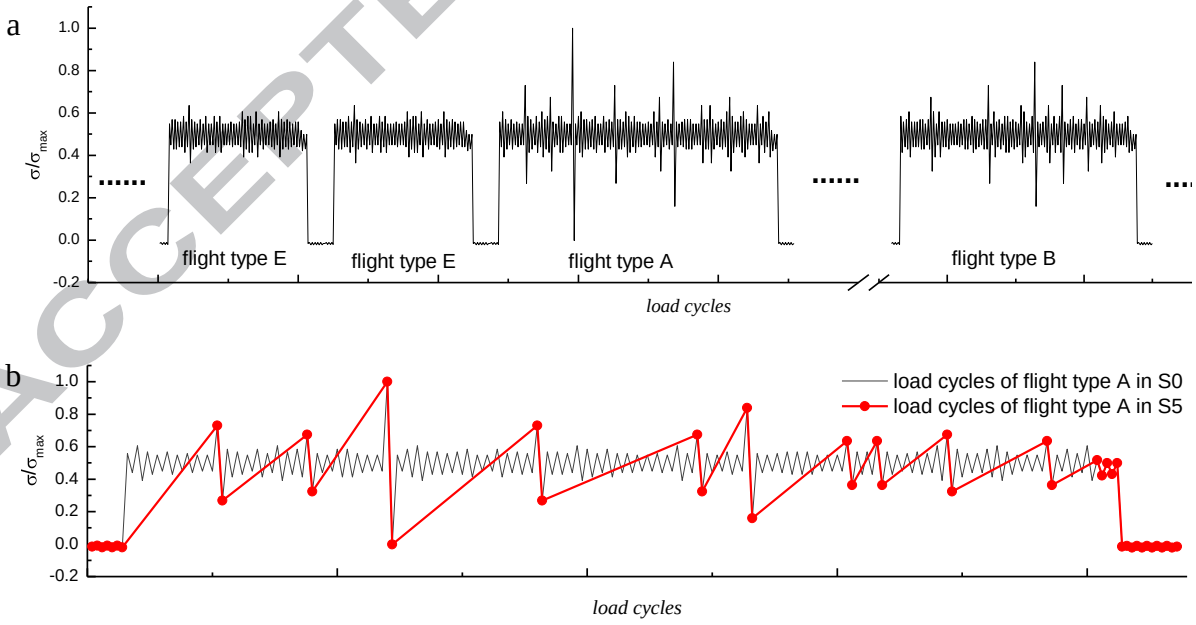

Fig. 2 Segments of the loading spectrum: (a) baseline spectrum, (b) load sequence of flight type A in S0 and S5.

ACCEPTED MANUSCRIPT

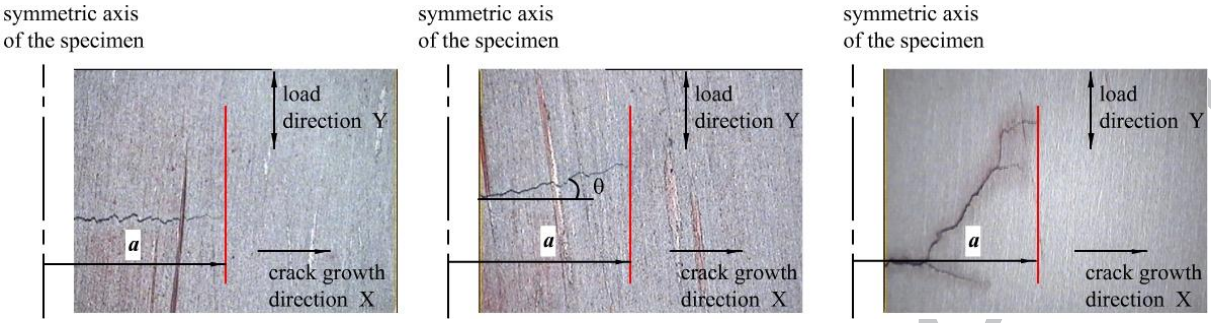

(a) (b) (c)

Fig. 3 Recorded crack lengths with respect to different crack morphologies.

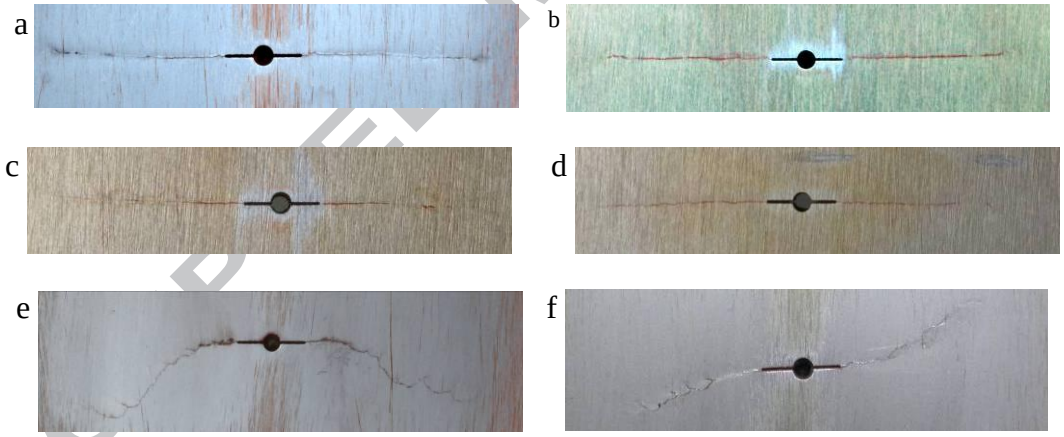

Fig.4 Crack morphologies under different loading spectra; (a), (b), (c), (d), (e) and (f) are for the S0, S1, S2, S3, S4 and S5 spectrum respectively.

ACCEPTED MANUSCRIPT

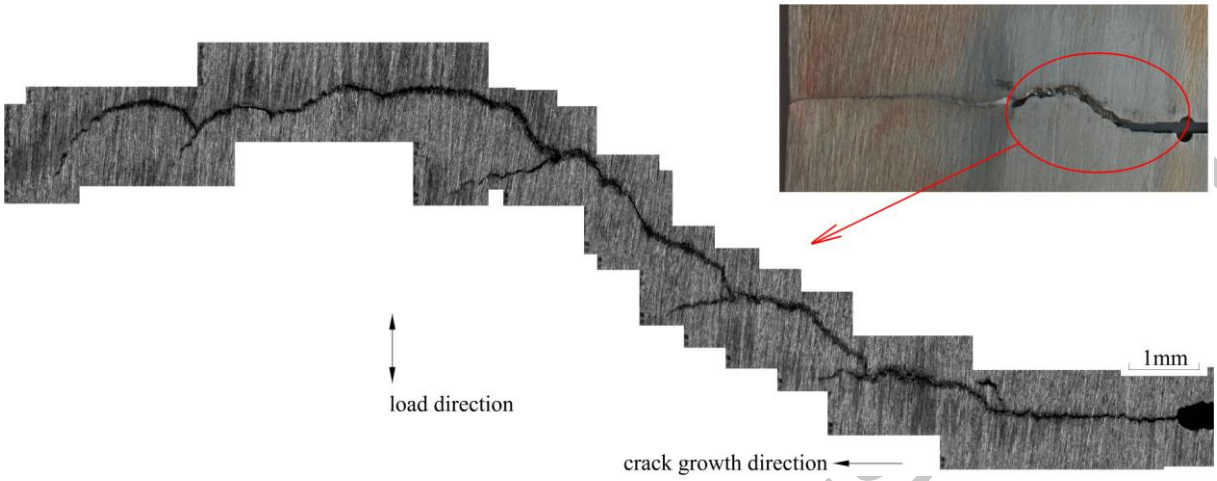

Fig. 5 Crack turning, meandering and branching for 2324-T39 (L-T) (the example shown here is under the spectrum S4 of low-load range truncation level of 17.11%)

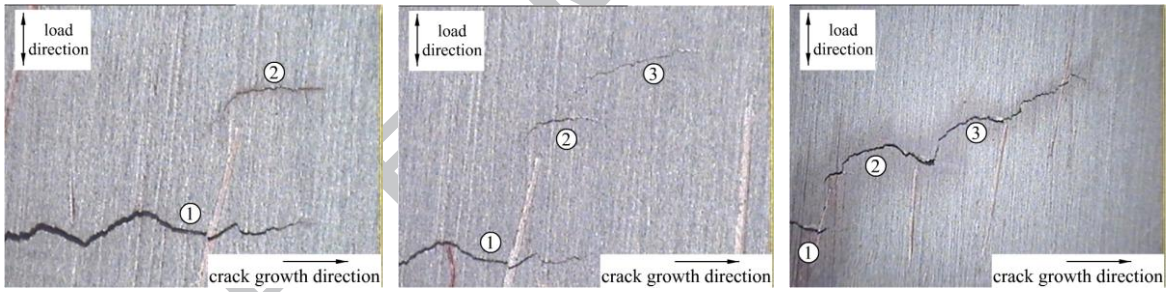

(a) (b) (c)

Fig. 6 Appearance of secondary surface cracks and cracks linking up (the example shown here is under the spectrum S5 of truncation level about 21.36%): (a) lead crack ①, secondary crack ②; (b) another secondary crack ③; (c) link-up of the two secondary cracks with the lead crack.

ACCEPTED MANUSCRIPT

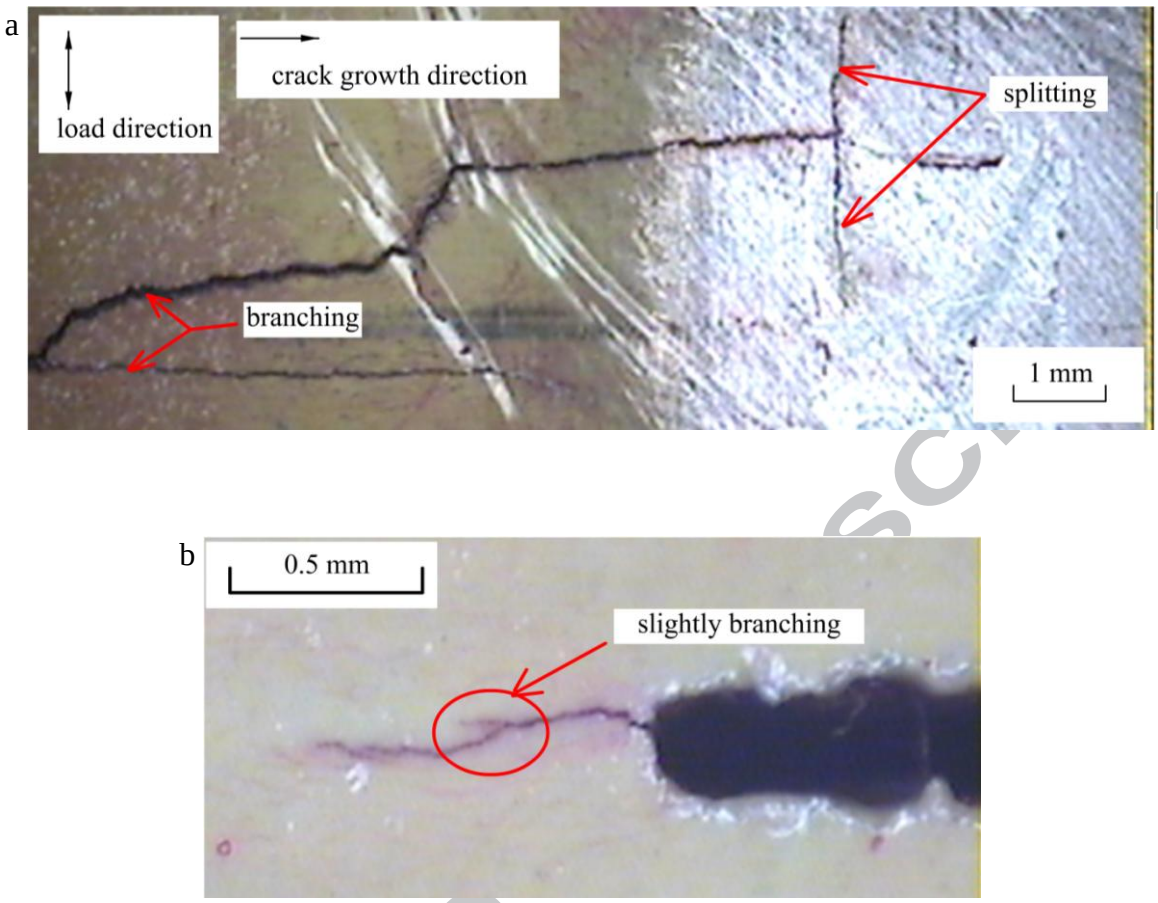

Fig. 7 Crack morphology of the L-S oriented 7050-T7451 specimens: (a) crack branching and splitting during propagation under spectrum S0, (b) crack branching during pre-cracking under constant amplitude loads.

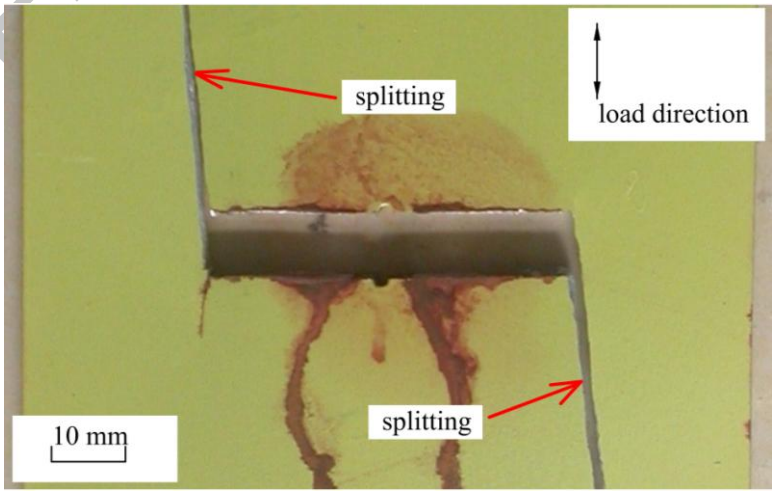

Fig. 8 Final splitting failure of a L-S oriented 7050-T7451 specimen under static residual strength test.

ACCEPTED MANUSCRIPT

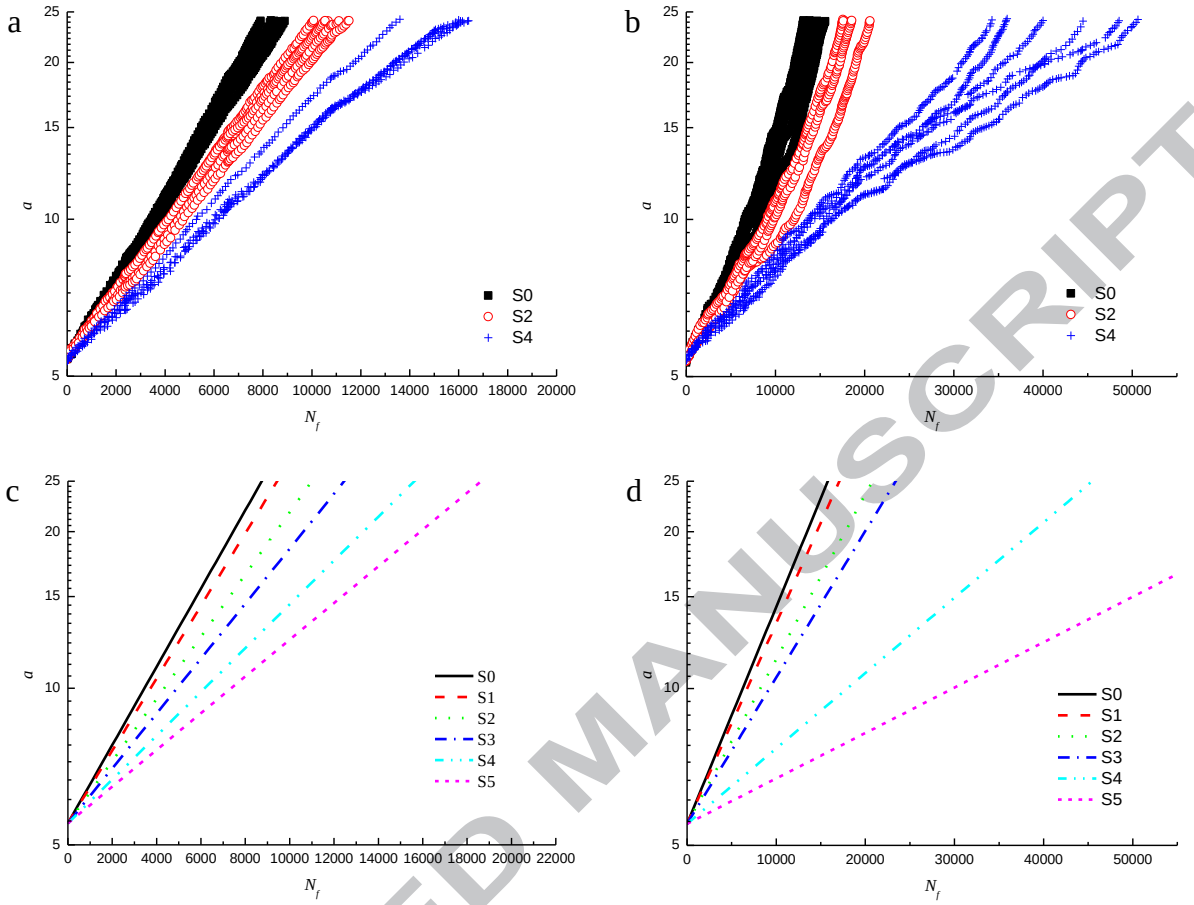

Fig.9 Test crack length vs. flights: (a), (b) are test raw data; (c), (d) are best fitting curves; (a), (c) are for 7050-T7451; (b), (d) are for 2324-T39.

ACCEPTED MANUSCRIPT

ACCEPTED MANUSCRIPT

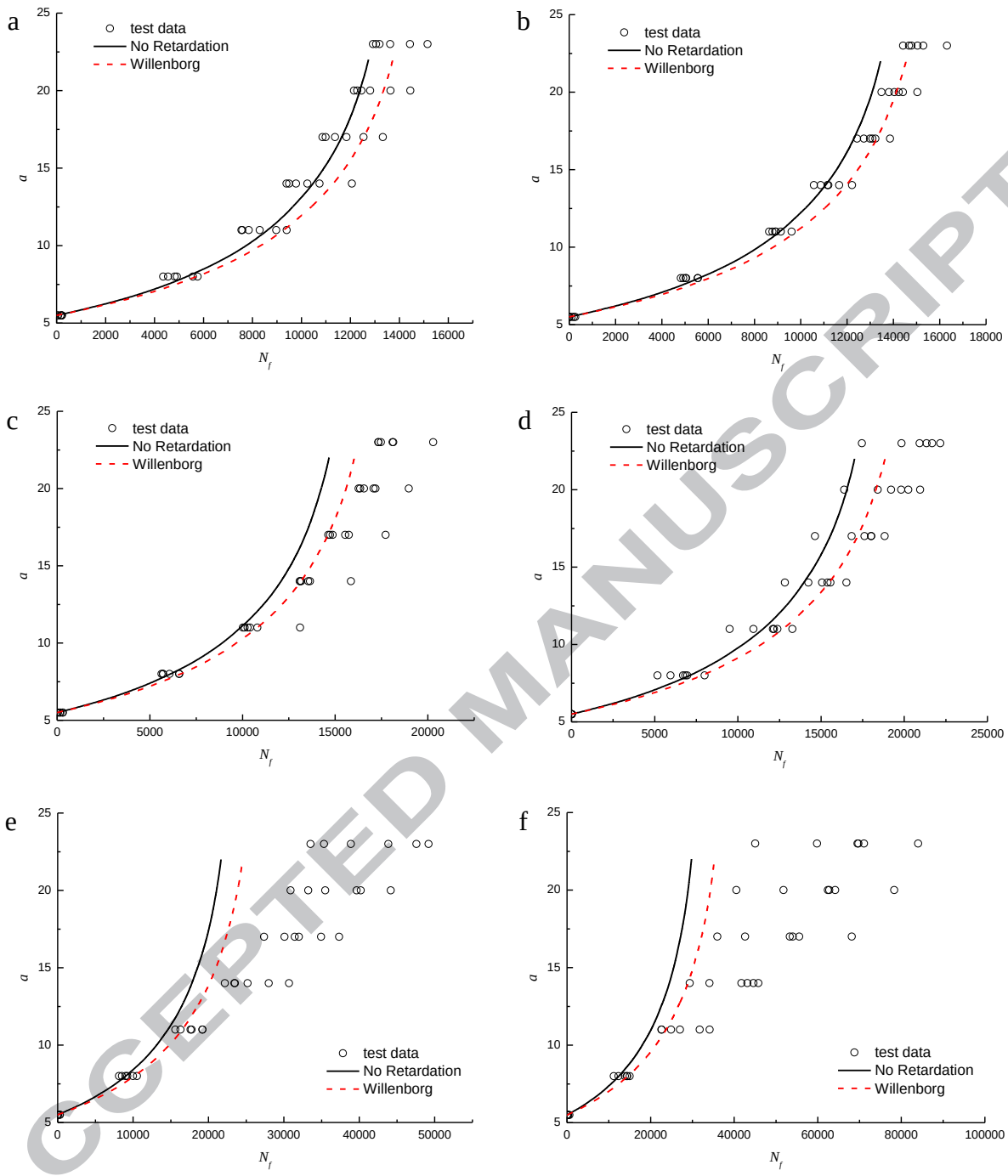

Fig. 10 Comparison of predicted a - N_f curve with the test data; (a), (b), (c), (d), (e) and (f) are for S0, S1, S2, S3, S4 and S5 spectrum, respectively.

ACCEPTED MANUSCRIPT

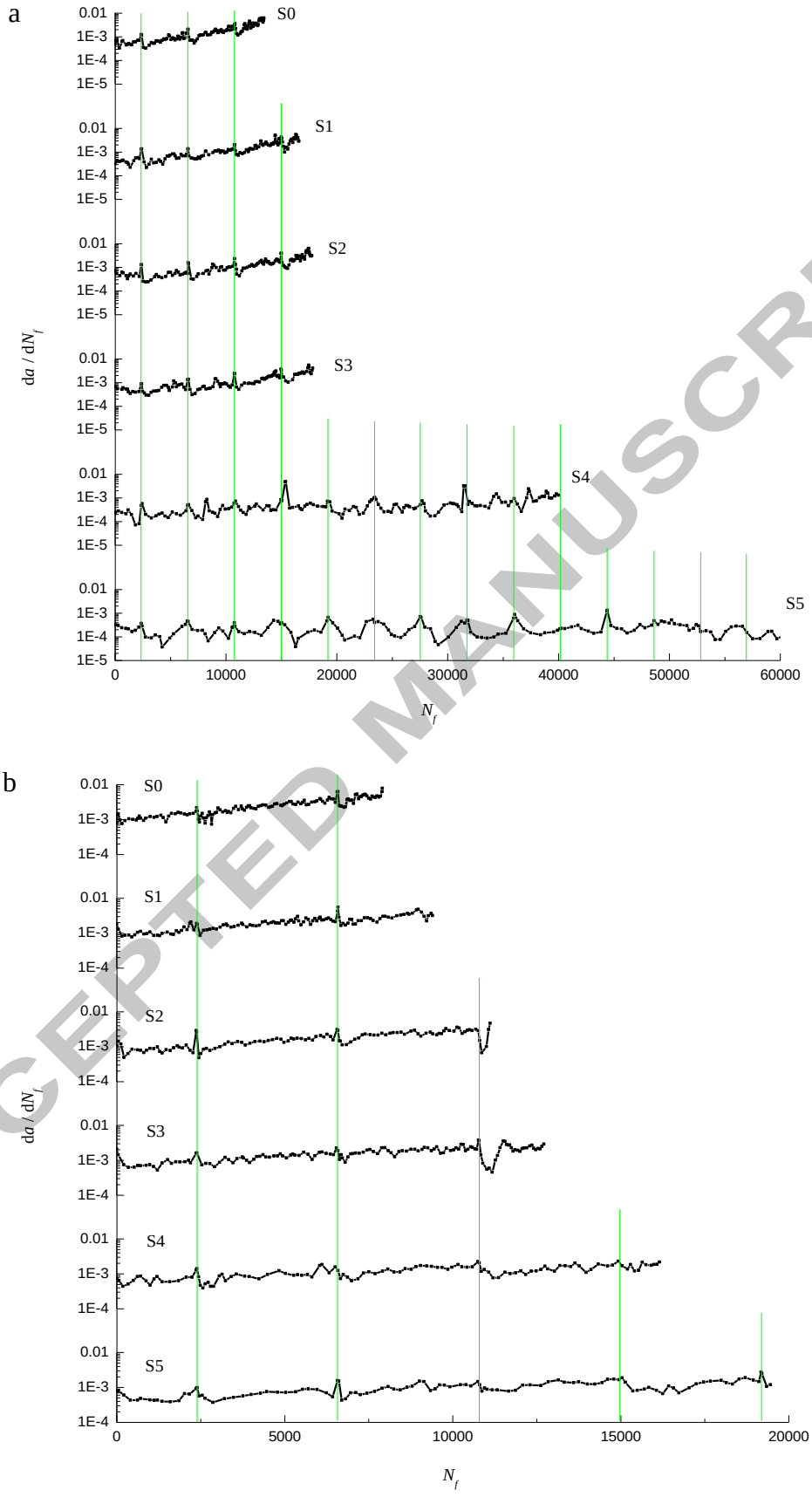

Fig. 11 Peak overload locations (vertical lines) and effect on crack growth rates: (a) AA 2324-T39, (b) AA 7050-T7451.

ACCEPTED MANUSCRIPT

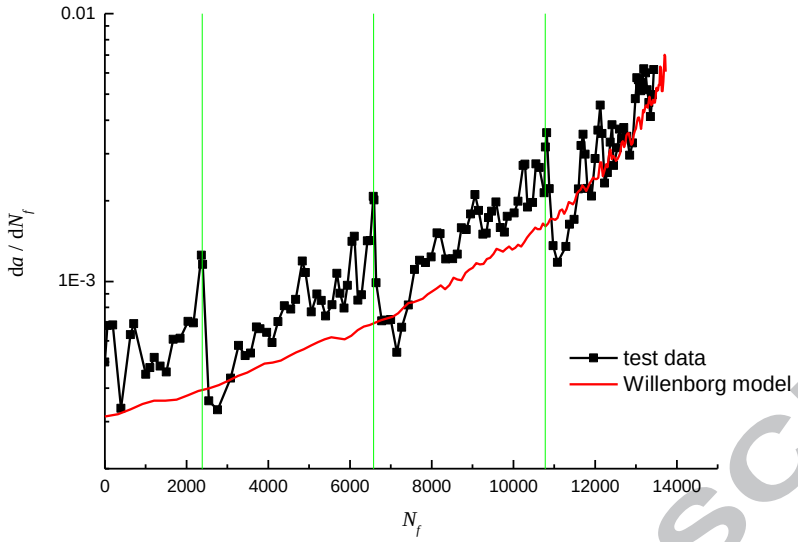

Fig. 12 Comparison of Willenborg retardation model and measured crack growth rate of Al 2324-T39 under S0.

ACCEPTED MANUSCRIPT